Experimental model of the pearlite interlamellar spacing in lamellar graphite iron

Vasilios Fourlakidis [1]*
Ilia Belov [1]
Attila Diószegi [1]

Abstract

The pearlite lamellar spacing ($\lambda_{pearlite}$) is one of the microstructure parameters that define the strength of the lamellar graphite iron (LGI). The transformation kinetics of $\lambda_{pearlite}$ has been the subject of several modeling studies for steels, which demonstrated that the $\lambda_{pearlite}$ can be calculated as a function of undercooling. However, it is hard to find in the literature the models for the prediction of $\lambda_{pearlite}$ in LGI. In the present work, $\lambda_{pearlite}$ in fully pearlitic LGI was investigated for a wide range of carbon contents and cooling rates. The undercooling and the cooling rates were estimated from the experimental cooling curves and were utilized for the prediction of $\lambda_{pearlite}$. The experimental data analysis provides an empirical expression that correlates $\lambda_{pearlite}$ and cooling rates from the eutectoid transformation region. The developed empirical model was incorporated into a casting simulation software to enable the prediction of $\lambda_{pearlite}$ in LGI and the simulation results were found to be in good agreement with the experimental data.

Keywords: Pearlite interlamellar spacing; Lamellar graphite iron; Eutectoid transformation.

1 Introduction

Usually, a fully pearlitic microstructure is required for the lamellar graphite iron (LGI) castings. Pearlite is a hard and brittle microstructural constituent and the pearlite lamellar spacing ($\lambda_{pearlite}$) has been reported to be the parameter primarily responsible for the strength characteristics in pearlitic steels. For fully pearlitic steels, the mechanical strength increases as the $\lambda_{pearlite}$ decreases [1,2]. Similar is believed to be the effect of pearlite refinement on the ultimate tensile strength of LGI [3-5]. It has been suggested in Fourlakidis et al. [6] that when a tensile force is applied on the LGI microstructure, multiple cracks form at the graphite lamellae tips and at a certain force level the cracks are propagated relatively easy through the interconnected graphite particles in the eutectic area. When one of the cracks reaches a pearlite colony that has been originated from the former primary austenite (dendrite structure), an additional force is required for the propagation of the crack. The magnitude of the additional force is proportional to the pearlite lamellar spacing. Additionally, $\lambda_{pearlite}$ has been employed in a modified Hall-Petch equation for the ultimate tensile strength prediction of LGI. Consequently, estimation of $\lambda_{pearlite}$ is an important step for modeling the mechanical properties of this alloy type.

Considering the similar morphology of the pearlite in steels and in cast iron it is assumed that the pearlite formation mechanism is similar for both alloys. The transformation of austenite to pearlite occurs by the nucleation and the cooperative growth of alternating ferrite and cementite lamellae that forms colonies having a single orientation. The most common parameter that characterizes pearlite is the interlamellar spacing ($\lambda_{pearlite}$), i.e. the distance between adjacent cementite lamellae in a colonies. The eutectoid transformation is a diffusion-controlled process and since the diffusion coefficient increases with temperature, at higher undercooling the lower temperature of reaction provides the smaller interlamellar spacing [7]. It is demonstrated in [8] that the $\lambda_{pearlite}$ is related to the pearlite growth rate, which is determined by the undercooling, regardless of the mode of transformation—isothermal, isovelocity, or continuous cooling. Based on the principles of interface diffusion-controlled growth and the maximum rate of entropy criterion, a relationship has been derived that correlates the minimum possible $\lambda_{pearlite}$ with the thermophysical parameters of interfacial energy of the ferrite–cementite interface, the change in enthalpy, the equilibrium temperature and the undercooling. Since the interfacial energy and the enthalpy change are relatively independent of the temperature the theoretical relations predict that $\lambda_{pearlite}$ and undercooling are inversely related [7]. Several empirical models have been developed for the prediction of $\lambda_{pearlite}$ in the pearlitic steels [8-11]. These models combine the effect of the alloying

elements with the thermophysical parameters involved in the interlamellar spacing selection.

The austenite to pearlite/ferrite transformation mode is extensively studied for the cast iron alloys [12,13], however, a limited number of researchers have investigated the contribution factors for the pearlite spacing selection in LGI. A linear relationship between the transformation temperature and the reciprocal lamellar spacing has been employed in Catalina et al. [3] for modeling $\lambda_{pearlite}$ in LGI. In a later study it has been suggested that $\lambda_{pearlite}$, in LGI is a function of the cooling rate at 800 °C and the content of Cu and Cr [14]. It has been shown that the refining of $\lambda_{pearlite}$ depends neither on the micro-segregation issued from the solidification step [15] nor on the austenite grain size [16], although the latter is disputed in Elwazri et al. [2]. Anyhow, it is likely that the pearlite fineness mainly depends on the cooling conditions during the eutectoid transformation and the alloying content.

In the present work the pearlite lamellar spacing is investigated for a wide range of carbon content and for different cooling rates typical for both thin and thick-walled complex shaped castings. The pearlite lamellar spacing is correlated with thermal data, obtained from the experiment, and an empirical expression is proposed that relates $\lambda_{pearlite}$ and cooling rates near the eutectoid transformation region.

2 Experimental methods

The experimental layout contained three cylindrical cavities each one surrounded by a different material (steel chill, sand and insulation material) intended to provide three different cooling rates. The entire assembly was enclosed by furan bounded sand mould. The dimensions of the cylinders surrounded by sand and chill were Ø50×70 mm and the insulated cylinder dimensions were Ø80×70 mm. A lateral 2-D heat flux condition was induced by placing an insulation plate at the top and the bottom of the cylindrical castings. The design of the cylindrical castings and arrangement of the experimental layout are shown in Figure 1.

Two type S thermocouples with glass tube protection were embedded in each cylindrical casting. A central thermocouple was located on the central axis of each cylinder. The distance between the central and the lateral thermocouples was 20 mm for the Ø50 mm cylinders and 30 mm for the Ø80 mm cylinder. The thermocouples were placed at the mid-height of each cylinder and the

temperatures were recorded at approximately 0.2 second interval. The cooling rates at the temperature intervals between 650 and 1250 °C of the metal in the chill, sand and insulation material were roughly 1.0, 0.3 and 0.1 °C/s, respectively. An electric induction furnace was utilized for melting of the charge material. The cast iron base alloy was inoculated with 0.4wt% of a standard Sr-based inoculant. Four hypoeutectic lamellar graphite iron heats with varying carbon contents were produced. The chemical compositions of the four different alloys are presented in Table 1. All the castings had a fully pearlitic microstructure (>90% pearlite).

The microstructure near the central thermocouple was analyzed. The microstructure specimens were color etched with a solution of picric acid, NaOH, KOH, and distilled water. The determination of the true lamellar spacing is complicated by the fact that not all the microstructure sectioning planes are perpendicular to the lamellae. Consequently, the observed spacing and thickness of the cementite lamellae can be larger than the real. Additionally, the real $\lambda_{pearlite}$, even for isothermally formed microstructure, is not constant but vary around the mean value [17]. In this work, a large area was scanned in the SEM and the average of the 10 smallest measurements were considered the correct spacing (perpendicular to the lamellae).

A CFD software FLOW-3D CAST [18] was employed to develop a full-scale 3D model of the casting process for the experimental layout. Simulation procedure consisted of model calibration with respect to the experimental cooling
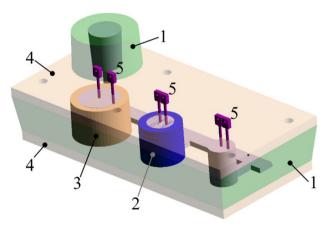

Figure 1. The experimental layout. (1) sand mould; (2) steel cylinder (chill); (3) cylindrical insulation material; (4) insulation plates; (5) thermocouples.

Table 1. Chemical composition (wt%) and carbon equivalent (C_{eq}=%C+%Si/3+%P/3)

Alloy	C	Si	Mn	P	S	Cr	Cu	C_{eq}
A	3.62	1.88	0.6	0.04	0.08	0.14	0.4	4.26
B	3.34	1.83	0.6	0.04	0.08	0.15	0.4	3.96
C	3.05	1.77	0.5	0.04	0.08	0.14	0.4	3.65
D	2.80	1.75	0.5	0.04	0.08	0.15	0.4	3.40

curves available at the location of the central thermocouple. Correct reproduction of the experimental cooling curves was the key for the $\lambda_{pearlite}$ computation methodology. In this work, the calibration was done by adjustment of the typical heat transfer coefficients between the metal and the insulation, sand and chill. The $\lambda_{pearlite}$ calculations for the cylinders were performed during post-processing. Detailed description of the simulation setup and procedure is presented in [19].

3 Results and discussion

The isothermal transformation temperature or the undercooling in steels and the cooling rate near the eutectoid region in the LGI are the parameters reported to have strong influence on $\lambda_{pearlite}$. These parameters were determined in this work from the data recorded for the central thermocouple. It has been demonstrated in [19] that the start of the phase transformation can be obtained from the cooling curve and its second derivative with respect to the time. The maximum of the second derivative indicates a sudden decrease in the cooling rate that corresponds to the beginning of the eutectic transformation. The same principle was utilized here for the determination of the undercooling during the eutectoid transformation. The cooling curve in the eutectoid transformation region of the A-alloy at the medium cooling rate, together with the second derivative of these data are presented in Figure 2.

The maximum of the second derivative coincides with the minimum eutectoid temperature in Figure 1, thus indicating the starting temperature for the formation of the pearlite, $T_{p,exp}$. The minimum eutectoid temperature has been also defined as the start temperature for the formation of pearlite in Alonso et al. [20]. Notice that the averaging smoothing technique (also known as mean filter) was implemented to the second derivative data and it could explain the small
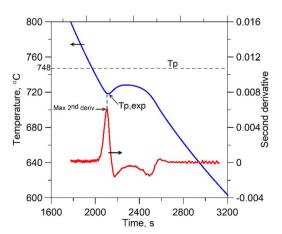
displacement of the second derivative maxima from the minimum eutectoid temperature.

The reference metastable temperature, T_p, is a function of the alloying content and can be estimated by Equation 1.

A thermodynamic software equipped with the appropriate database was employed to derive Equation 1. The calculations were performed for up to 3 wt% Si, up to 1 wt% Mn, Cu, Cr and Ni and up to 0.5 wt% Mo content [21]:

$$Tp = 727 + 21.6 \cdot w_{Si} + 0.023 \cdot (wsi)^2 - 21 \cdot w_{Cu} - 25 \cdot w_{Mn} + 8 \cdot w_{Mo} + 13 \cdot w_{Cr} - 33 \cdot w_{Ni} + 21 \cdot w_{Sn} \tag{1}$$

where the temperature is in °C and the alloying content in wt%.

The nominal content of each element should be multiplied by 1.05 to account for the presence of graphite.

The temperature T_p of the experimental alloys is found to be 748 °C for alloy A, 747 °C for alloy B and 746 °C for alloys C and D. The undercooling, $\Delta T = T_p - T_{p,exp}$, and the cooling rate dT/dt in the temperature interval between 750 and 760 °C, were calculated. The temperature interval, for the estimation of the cooling rate was chosen to be near $T_{p,exp}$ and at the same time, it was aimed to remain within the temperature interval where the second derivative is constant.

The effect of the undercooling and the cooling rate between 750 and 760 °C on $\lambda_{pearlite}$ is seen in Figures 3 where, as expected, $\lambda_{pearlite}$ decreases with increased absolute value of the cooling rate and decreased undercooling. There is a strong correlation between the absolute value of cooling rate and $\lambda_{pearlite}$ as can be seen from Figure 3b.

Regression analyses was performed on the experimental data and Equation 2 and Equation 3 were obtained for the prediction of $\lambda_{pearlite}$ in µm. Due to the much higher correlation coefficient (R^2), Equation 3 is considered sufficient for the prediction of $\lambda_{pearlite}$:

$$\lambda_{pearlite} = 0.87 + 0.02 \cdot \Delta T \tag{2}$$

$$\lambda_{pearlite} = 0.124 \cdot \left(\frac{dT}{dt} [750 - 760°C] \right)^{-0.46} \tag{3}$$

Based on the kinetics theories of the decomposition of austenite to pearlite, Equation 4 has been derived in [7] where the $\lambda_{pearlite}$ is determined as a function of the interfacial energy between ferrite and cementite within the pearlite, $\sigma_{\alpha/\theta}$, the change in enthalpy, ΔH, and the undercooling, ΔT:

$$\lambda_{pearlite} = \frac{4 \cdot \sigma_{\alpha/\theta} \cdot T_P}{\Delta H \cdot \Delta T} \tag{4}$$

For $\sigma_{\alpha/\theta}$ equal to 1 J/m^2 and ΔH equal to 8.0×10^8 J/m^3 [22], $\lambda_{pearlite}$ was calculated for the undercooling range examined in this work and the results are plotted in Figure 3a (dashed line). As can be seen the $\lambda_{pearlite}$ values calculated from

Figure 2. Cooling curve and its second derivative for alloy A and for the medium cooling rate (Sand).
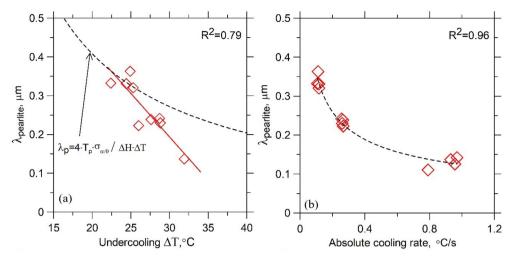
Figure 3. (a) Interlamellar spacing as a function of undercooling; (b) Interlamellar spacing as a function of cooling rate at the temperature interval between 750 °C and 760 °C.
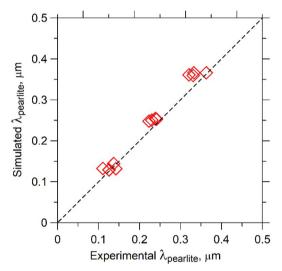

Figure 4. Correlation between measured and simulated $\lambda_{pearlite}$ values.

Equation 4, coincide with the experimental values of the lower cooling rate meaning that the theoretical equation is more suitable for cooling conditions that approach the thermodynamic equilibrium.

The alloying elements are reported to influence $\lambda_{pearlite}$ in pearlitic steels. Increased content of Cr, Mo, C and Si results in decreased $\lambda_{pearlite}$. Contrary, the $\lambda_{pearlite}$ increases with increased content of Ni and Mn [23].

The addition of Cr and Cu refines the pearlite of LGI [4]. The carbon content was the only element content that varied in this study. The experimental results showed that the effect of carbon on the $\lambda_{pearlite}$ was insignificant in comparison to the cooling rate.

The simulated cooling rates at the temperature interval between 750 and 760 °C were used in Equation

2 for the calculation of $\lambda_{pearlite}$. Comparisons between the calculated and the measured data are demonstrated in Figure 4. The graph reveals a strong correlation between the measured and computed $\lambda_{pearlite}$. The eutectoid reaction model in the simulation employed the enthalpy method [19], therefore the undercooling was not predicted. For this reason, it was not possible to calculate $\lambda_{pearlite}$ from Equation 2.

4 Conclusions

A wide range of carbon content and cooling rates were utilized in this work, for the production of fully pearlitic LGI. Data from the thermal analysis and the microstructure investigation were correlated to generate empirical models for the prediction of $\lambda_{pearlite}$. The results show that the cooling rate, rather than the undercooling, is the most suitable parameter for the prediction of $\lambda_{pearlite}$.

The developed model was incorporated in a casting simulation software to enable the prediction of $\lambda_{pearlite}$ in LGI. The results shows that there is a good agreement between the calculated and the experimental data.

References

1   Marder AR, Bramfitt BL. The effect of morphology on the strength of pearlite. MTA. 1976;7(3):365-372.

2   Elwazri AM, Wanjara P, Yue S. The effect of microstructural characteristics of pearlite on the mechanical properties of hypereutectoid steel. Materials Science and Engineering A. 2005;404(1-2):91-98.

3   Catalina A, Guo X, Stefanescu DM, Chuzhoy L, Pershing MA. Prediction of room temperature microstructure and mechanical properties in lamellar iron castings. AFS Trans. 2000;94:889-912.

4   Sjögren T, Svensson H. Study of the eutectoid transformation in grey cast irons and its effect on mechanical properties. Key Engineering Materials. 2010;457:157-162.

5   Fourlakidis V, Diószegi A. A generic model to predict the ultimate tensile strength in pearlitic lamellar graphite iron. Materials Science and Engineering A. 2014;618:161-167.

6   Fourlakidis V, Diaconu L, Diószegi A. Strength prediction of Lamellar Graphite Iron: from Griffith's to Hall-Petch modified equation. Trans Tech Publications. 2018;925:272-279.

7   Mehl RF, Hagel WC. The austenite: pearlite reaction. Progress in Metal Physics. 1956;6:74-134.

8   Marder AR, Bramfitt BL. Effect of continuous cooling on the morphology and kinetics of pearlite. MTA. 1975;6(11):2009-2014.

9   Caballero FG, Capdevila C, Garcia de Andres C. Modeling of the interlamellar spacing of isothermally formed pearlite in a eutectoid steel. Cripta Materialia. 2000;42(6):537-542.

10 Pernach M. Application of the mixed-mode model for numerical simulation of pearlitic transformation. Journal of Materials Engineering and Performance. 2019;28(5):3136-3148.

11 Takahashi M. Reaustenitization from bainite in steels [thesis]. Cambridge: University of Cambridge; 1992.

12 Lacaze J. Pearlite growth in cast irons: a review of literature data. International Journal of Cast Metals Research. 1999;11(5):431-436.

13 Stefanescu DM. Modeling of cast iron solidification: the defining moments. Metallurgical and Materials Transactions. A, Physical Metallurgy and Materials Science. 2007;38:1433-1447.

14 Svensson H, Sjögren T. The effect of cooling rate, section size and alloying on matrix structure formation in pearlitic grey cast iron. Key Engineering Materials. 2010;457:169-174.

15 Freulon A, Sertucha J, Lacaze J. Solidification and room temperature microstructure of a fully pearlitic compacted graphite cast iron. Transactions of the Indian Institute of Metals. 2018;71(11):2651-2656.

16 Aranda MM, Kim B, Rementeria R, Capdevila C, de Andrés CG. Effect of Prior Austenite Grain Size on Pearlite Transformation in a Hypoeuctectoid Fe-C-Mn Steel. Metallurgical and Materials Transactions. A, Physical Metallurgy and Materials Science. 2014;45(4):1778-1786.

17 Pellissier GE. The interlamellar spacing of pearlite. Trans. ASM. 1942;30:1049-1086.

18 Barkhudarov MR, Hirt CW. Casting simulation: mold filling and solidification: benchmark calculations using FLOW-3D. Santa Fe, NM: Flow Science, Inc.; 1993. (Technical report) [cited 2021 Sept. 2]. Available at: https://www.flow3d.com/wp-content/uploads/2014/08/Casting-Simulation-Mold-Filling-and-Solidification-Benchmark-Calculations-Using-FLOW-3D.pdf

19 Fourlakidis V, Belov I, Diószegi A. Strength prediction for pearlitic lamellar graphite iron: model validation. Metals. 2018;8(9):684.

20 Alonso G, Larrañaga P, Sertucha J, Suárez R, Stefanescu DM. Gray cast iron with high austenite-to-eutectic ratio part I- calculation and experimental evaluation of the fraction of primary austenite in cast iron. Trans. AFS. 2012;120:329-335.

21 Sertucha J, Larrañaga P, Lacaze J, Insausti M. Experimental investigation on the effect of copper upon eutectoid transformation of as-cast and austenitized spheroidal graphite cast iron. Inter Metalcast. 2010;4(1):51-58.

22 Kramer JJ, Pound GM, Mehl RF. The free energy of formation and the interfacial enthalpy in pearlite. Acta Metallurgica. 1958;6(12):763-771.

23 Ridley N. A review of the data on the interlamellar spacing of pearlite. MTA. 1984;15(6):1019-1036.